The Gravitational Wave Portal to Neutrino Mass Mechanisms

Andrea Addazi,[1,*] Antonino Marcianò,[1,†] António P. Morais,[2,‡]
Roman Pasechnik,[3,§] Rahul Srivastava,[4,¶] and José W. F. Valle[4,**]

[1] *Department of Physics & Center for Field Theory and Particle Physics, Fudan University, 200433 Shanghai, China*
[2] *Departamento de Física, Universidade de Aveiro and CIDMA, Campus de Santiago, 3810-183 Aveiro, Portugal*
[3] *Department of Astronomy and Theoretical Physics, Lund University, 221 00 Lund, Sweden*
[4] *AHEP Group, Institut de Física Corpuscular – C.S.I.C./Universitat de València, Parc Científic de Paterna. C/ Catedrático José Beltrán, 2 E-46980 Paterna (Valencia) - SPAIN*

We present a detailed phenomenological analysis of the primordial gravitational-wave (GW) radiation that emerges from the strong first-order electroweak phase transition, as a probe of neutrino mass models. We focus on transitions and the corresponding GW spectra that relate to simple variants of the seesaw mechanism that both entail "high-scales" as well as "low-scales", encoding either explicit or spontaneously broken lepton number symmetry. In particular, low-scale realizations, known as the inverse seesaw, are identified as suitable theory setups for producing strong first-order electroweak phase transitions, if lepton number violation arises spontaneously. The resulting Nambu-Goldstone boson, the so-called majoron, may then also play the role of cosmological Dark Matter in this scenario. The models encoding majorons entail strong first order phase transitions (FOPTs), and non-trivial primordial GW spectra. These latter may unravel precious phenomenological signatures within the frequency and amplitude sensitivity range of upcoming experiments, among which LISA, BBO and u-DECIGO. Investigating several FOPTs associated to different models for neutrino mass generation, we were able to realize that there are cases in which the resulting GW spectra are characterized by double or multiple peaks. This is a feature that can be resolved in forth- coming experiments. The majoron variants of the low-scale seesaw mechanism we analyzed imply different GW spectra than the ones predicted within the framework of the high-scale majoron seesaw. This is another testable feature for forthcoming experiments. Our analysis endorses GWs signal as a powerful and complementary portal to be deployed in order to test the neutrino mass sector.

I. INTRODUCTION

Color Code RED: To be changed/removed/improved
Color Code BLU: Antonino

Non-zero neutrino masses constitute one of the most robust evidences for new physics [1, 2]. Despite the great efforts over the last two decades to underpin the origin of neutrino mass, the basic underlying mechanism remains as elusive as ever. It has recently been advocated that the spectrum of primordial gravitational waves (GWs) potentially measurable at the currently planned GW interferometers represents an important new probe for new physics due its particular sensitivity to the details of the electroweak phase transition epoch in the cosmological history [3]. A dynamical understanding of neutrino mass generation necessarily introduces new scalar multiplets. A paradigmatical approach is provided by the seesaw mechanism [4], in which neutrinos owe their small mass to the exchange of

* andrea.addazi@lngs.infn.it
† marciano@fudan.edu.cn
‡ aapmorais@ua.pt
§ Roman.Pasechnik@thep.lu.se
¶ rahulsri@ific.uv.es
** valle@ific.uv.es

heavy mediators. In its canonical high-scale realization, the seesaw mechanism will not affect the electroweak phase transition (EWPT) in any substantial way, even if new dynamics in the scalar sector is invoked. However, the physics responsible for neutrino masses could lie at a low scale [5, 6]. In particular, the seesaw mechanism can be realized at low scale [7–11]. The models are not only theoretically attractive but also of great phenomenological interest for particle physics measurements as well as cosmology and astrophysics. In this case one expects to that the nature of the electroweak phase transition (EWPT) can be modified in a substantial way [12].

In this work, we study the details of the EW phase transition and the emergence of primordial GWs within low-scale seesaw mechanism. For simplicity here we focus on the case of the inverse seesaw model with ungauged lepton number symmetry [7, 8]. This is a simple extension of the standard model with a minimally extended scalar sector containing, besides the Higgs $SU(2)$ doublet, also a complex $\mathrm{SU(3)_c} \otimes \mathrm{SU(2)_L} \otimes \mathrm{U(1)_Y}$ singlet scalar. The model implements spontaneous lepton number violation and hence has a Nambu-Golstone boson, the so-called majoron, a CP-odd light scalar with important cosmological implications associated to Dark Matter [13–19]. In addition to the heavy TeV-scale neutrinos and the majoron, the physical spectrum contains a second Higgs-like CP-even state mixed with the standard model Higgs boson potentially modifying the couplings of the 125 GeV standard model Higgs that can be probed in collider measurements [20–22]. Moreover, these models can also lead to many other implications such as potentially large effects in the propagation of astrophysical neutrinos [23–27], lepton number violation processes such as $0\nu\beta\beta$decay [28], as well as lepton flavor violation and collider processes [29–35]. Regions of the inverse seesaw parameter space that are currently inaccessible to particle physics experiments may also lead to interesting astrophysics and cosmology. For example, its relatively light neutrino mass mediators, close to the EW scale, could significantly affect the dynamics of the EW phase transition via Yukawa interactions with a low-scale scalar sector containing the standard model Higgs boson.

The paper is organised as follows...

II. PHASE TRANSITIONS

Let us begin with a general discussion of phase transitions in quantum field theory and how the signatures of violent first order phase transitions (F.O.P.Ts) can be embedded in the resulting gravitation waves. At high temperatures, phase transitions (PTs) may occur through thermal jumps, while at low temperatures they are dominated by quantum tunneling. The latter are realised as non-perturbative solutions of the equations of motion, well-known as instantons [36, 37]. Both cases are treated within the same formalism based upon a description of classical motion in Euclidean space by means of the action [38].

$$\hat{S}_3(\hat{\phi}, T) = 4\pi \int_0^\infty \mathrm{d}r\, r^2 \left\{ \frac{1}{2} \left(\frac{\mathrm{d}\hat{\phi}}{\mathrm{d}r} \right)^2 + V_{\mathrm{eff}}(\hat{\phi}, T) \right\} , \tag{1}$$

where $\hat{\phi}$ is a solution of the equation of motion which is usually found by calculating the path that minimizes the energy of the field (for more details, see e.g. Refs. [38, 39]).

The temperature of the phase transition is typically identified with the bubble nucleation temperature, T_n, at which the probability of one transition per cosmological horizon volume is of order one [**?**], i.e.

$$\int_0^{t_n} \Gamma\, V_H(t)\, dt = \int_{T_n}^\infty \frac{dT}{T} \Big(\frac{2\zeta M_{\mathrm{Pl}}}{T} \Big)^4 e^{-\hat{S}_3/T} = \mathcal{O}(1) , \tag{2}$$

where $V_H(t)$ is the volume of the cosmological horizon, $\zeta \sim 3 \cdot 10^{-3}$, M_{Pl} is the Planck scale, and

$$\Gamma \sim A(T) e^{-\hat{S}_3/T} , \qquad A(T) = \mathcal{O}(T^4) . \tag{3}$$

is the tunneling rate per unit time per unit volume [**?**]. The condition (2) numerically translates to the following equation [37]

$$\frac{\hat{S}_3(T_n)}{T_n} \sim 140\,. \tag{4}$$

Then the basic criterion for the strong first-order EW phase transitions relevant for efficient production of gravitation waves reads [40]

$$\frac{v_h(T_n)}{T_n} \gtrsim 1\,, \tag{5}$$

where $v_h(T_n)$ is the Higgs VEV value at $T = T_n$.

When degenerate minima in the effective potential occur, the nucleation temperature can be much smaller than the critical temperature, T_c. This corresponds to supercooling, a common phenomenon for strong first-order phase transitions. If Eq. (4) does not have any solutions, then transitions do not occur during the thermal history of the Universe [40], although they may still eventually happen at asymptotically large times and at $T = 0$ via tunneling. In this work, we do not discuss the latter case and focus only on phase transitions happening at sufficiently large T when nontrivial solutions of equation 4 exist. We will compute the nucleation temperature within high and low-scale realizations of the type I seesaw. We will also consider the majoron variants of the seesaw mechanism. The phase transition is studied using the `CosmoTransitions` package [39].

In order to compute the properties of the EW and lepton number violation phase transitions relevant for the primordial GWs production mechanism we will be studying tunneling probabilities and nucleation temperatures which require a detailed analysis of the effective potential away from its minima. As was already argued in Ref. [**?**], the corresponding results do not depend strongly on the gauge choice even though this standard treatment is, in general, not gauge-invariant. A gauge-invariant implementation of the daisy resummation in the minimum of the effective potential has been performed in Ref. [**?**]. An analogous analysis in the fully gauge-invariant approach outside of the minima goes beyond the scope of the present work.

III. LINKING GRAVITATIONAL WAVES SPECTRUM TO THE EFFECTIVE POTENTIAL

An important signature of such violent out-of-equilibrium cosmological processes as the PTs is the associated stochastic primordial GWs. The corresponding power spectrum [12, 41]

$$h^2\Omega_{\rm GW}(f) \equiv \frac{h^2}{\rho_c}\frac{\partial\rho_{\rm GW}}{\partial\log f}\,, \tag{6}$$

where ρ_c is the critical energy density today, which has three relevant components [42],

$$h^2\Omega_{\rm GW} \simeq h^2\Omega_{\rm coll} + h^2\Omega_{\rm SW} + h^2\Omega_{\rm MHD}\,, \tag{7}$$

emerging due to (i) collisions between the bubble walls [43], $\Omega_{\rm coll}$, (ii) subsequent sound wave echoes [44], $\Omega_{\rm SW}$, and (iii) the associated magnetohydrodynamic turbulences in the cosmological plasma [45], $\Omega_{\rm MHD}$.

A detailed knowledge of the effective potential $V_{\rm eff}(\phi_\alpha; T)$ is important in order to obtain the key parameters of the primordial GWs power spectrum, such as the inverse time-scale β of the PT, represented in units of the Hubble parameter H,

$$\frac{\beta}{H} = T_n\,\frac{\partial}{\partial T}\left(\frac{\hat{S}_3}{T}\right)\bigg|_{T_n}\,, \tag{8}$$

and the latent heat α released during the PT relative to the energy density of the Universe,

$$\alpha = \frac{1}{\rho_\gamma}\Big[V_i - V_f - T\Big(\frac{\partial V_i}{\partial T} - \frac{\partial V_f}{\partial T}\Big)\Big]\,, \tag{9}$$

where T_n is the nucleation temperature, $\hat{S}_3$ is the Euclidean action introduced in the previous section, V_i and V_f are the initial (metastable phase) and final (stable phase) values of the effective potential, and ρ_γ is the energy density of the radiation medium at the nucleation epoch. For the case of the EWPT it is found as

$$\rho_\gamma = g_*\frac{\pi^2}{30}T_n^4\,, \qquad g_* \simeq 106.75\,, \tag{10}$$

in terms of the number of relativistic d.o.f.'s. For each of the contributions in Eq. (7), the corresponding GW signals are found schematically as

$$\text{signal} \;\sim\; \text{amplitude} \;\times\; \text{spectral shape}\;(f/f_{\rm peak})\,, \tag{11}$$

where f is the GW frequency, and $f_{\rm peak}$ is the peak-frequency. Detailed expressions for each of the three sources in terms of β/H and α quantities used in our computation of the GWs power spectrum can be found in Refs. [12, 41, 42] and are given also in Section IV, for an easy reference.

IV. SOURCES OF PRIMORDIAL GRAVITATIONAL WAVES PRODUCTION

Here, we briefly discuss the standard formalism used in our computations of the GWs spectrum in Eq. (7). Gravitationl waves originate from the three main sources: (i) bubble wall collisions, (ii) sound waves, and (iii) magnetohydrodynamic turbulences. Below, we list the corresponding semi-analytical expressions for the GW spectrum obtained as best fit with model-independent numerical simulations. For more details, see e.g. Ref. [46] and references therein.

Bubble wall collisions contribution

This contribution is treated in the envelope approximation [42]. The peak frequency is found as follows

$$f_{\rm coll}[\text{Hz}] = 1.65\times10^{-5}\frac{0.62}{v_b^2 - 0.1v_b + 1.8}\frac{\beta}{H}\left(\frac{T_n}{100\,\text{GeV}}\right)\left(\frac{g_*}{100}\right)^{1/6}\,, \tag{12}$$

in terms of the nucleation temperature, T_n, relative inverse time-scale of the phase transition, β/H found in Eq. (**??**), and the bubble wall velocity, v_b, found for supersonic bubbles in terms of the relative latent heat α computed in Eq. (**??**) as follows [12]

$$v_b = \frac{1/\sqrt{3} + \sqrt{\alpha^2 + 2\alpha/3}}{1+\alpha}\,. \tag{13}$$

The corresponding energy density reads

$$h^2\Omega_{\rm coll}(f) = 1.67\times10^{-5}\left(\frac{\beta}{H}\right)^{-2}\left(\frac{\kappa\alpha}{1+\alpha}\right)^2\left(\frac{g_*}{100}\right)^{-1/3}\frac{0.11v_b^3}{0.42+v_b^2}\left(\frac{f}{f_{\rm coll}}\right)^{2.8}\frac{3.8}{1+2.8(f/f_{\rm coll})^{3.8}}\,, \tag{14}$$

where κ is the efficiency factor defined as a fraction of released latent heat deposited in a thin shell close to the phase transition front. In the so-called envelop approximation, the efficiency κ is taken to be equal to the fraction of the latent heat transformed into the kinetic energy of the scalar fields κ_ϕ defined below.

Sound waves contribution

For the second source of GWs from sound waves, the peak frequency of the GW spectrum the has the following semi-analytical parametrization

$$f_{\rm SW}[{\rm Hz}] = 1.9\times10^{-5}\frac{\beta}{H}\frac{1}{v_b}\left(\frac{T_n}{100\,{\rm GeV}}\right)\left(\frac{g_*}{100}\right)^{1/6}, \tag{15}$$

such that the energy density of the GWs is found as

$$h^2\Omega_{\rm SW}(f) = 2.65\times10^{-6}\left(\frac{\beta}{H}\right)^{-1}\left(\frac{\kappa_v\alpha}{1+\alpha}\right)^2\left(\frac{g_*}{100}\right)^{-1/3}v_b\left(\frac{f}{f_{\rm SW}}\right)^3\left(\frac{7}{4+3(f/f_{\rm SW})^2}\right)^{7/2}, \tag{16}$$

where κ_v is the efficiency factor determined as the fraction of latent heat transformed into bulk motion of the fluid (see Eqs. (22) and (23) below).

MHD turbulence contribution

In this case the peak frequency is

$$f_{\rm MHD}[{\rm Hz}] = 2.7\times10^{-5}\frac{\beta}{H}\frac{1}{v_b}\left(\frac{T_n}{100\,{\rm GeV}}\right)\left(\frac{g_*}{100}\right)^{1/6} \tag{17}$$

The energy density is

$$h^2\Omega_{\rm MHD}(f) = 3.35\times10^{-4}\left(\frac{\beta}{H}\right)^{-1}\left(\frac{\kappa_{\rm turb}\alpha}{1+\alpha}\right)^{3/2}\left(\frac{g_*}{100}\right)^{-1/3}v_b\left(\frac{f}{f_{\rm MHD}}\right)^3\left(\frac{(1+f/f_{\rm MHD})^{-11/3}}{1+8\pi f/h_*}\right) \tag{18}$$

where $\kappa_{\rm turb}$ is the efficiency factor determined as the fraction of latent heat transformed into MHD turbulence (vorticity) that differs from κ_ϕ and κ_v in the case of bubble wall collisions and sound waves described above, respectively. Following Ref. [**?**], we take

$$\kappa_{\rm turb} = \epsilon\kappa_v\,, \tag{19}$$

where $\epsilon\simeq0.05$ is the turbulence efficiency defined as the fraction of the bulk motion which is turbulent, and

$$h_*[{\rm Hz}] = 1.65\times10^{-5}\left(\frac{T_n}{100\,{\rm GeV}}\right)\left(\frac{g_*}{100}\right)^{1/6}. \tag{20}$$

Efficiencies: non-runaway vs runaway bubbles

For *non-runaway bubbles*, the collision term (14) is small, so the dominant contributions to the GWs energy spectrum come from sound waves, Eq. (16), and the MHD turbulence effect, i.e.

$$h^2\Omega_{\rm GW}\simeq h^2\Omega_{\rm SW}+h^2\Omega_{\rm MHD}\,, \tag{21}$$

In the case of non-runaway but still supersonic bubbles with $v_b\sim1$, the efficiency factor Eq. (16) is given by [42]

$$\kappa_v = \frac{\alpha}{0.73+0.083\sqrt{\alpha}+\alpha}\,, \tag{22}$$

while for slow bubble walls, $v_b\lesssim0.1$, another parameterisation applies

$$\kappa_v = \frac{v_b^{6/5}\,6.9\alpha}{1.36-0.037\sqrt{\alpha}+\alpha}\,. \tag{23}$$

The *runaway bubbles* expanding in the cosmological plasma correspond to unbounded acceleration of the bubble wall $v_b \to 1$ as α increases. The bubble wall collisions cannot be neglected any longer, so that each of the three sources in Eq. (7) are relevant. For α above its smallest value α_∞, for which the bubbles are still runaway, the fraction of the total PT energy budget deposited into the fluid saturates. The energy surplus parameterized by the fraction

$$\kappa_\phi = 1 - \frac{\alpha_\infty}{\alpha}\,, \tag{24}$$

goes into acceleration of the bubble wall and determines the bubble wall collisions contribution (14), so that only α_∞/α fraction of the total energy budget is transformed into the bulk motion. The corresponding efficiency factor becomes smaller than for non-runaway case and takes the form

$$\kappa_v = \frac{\alpha_\infty}{\alpha}\kappa_\infty\,, \qquad \kappa_\infty = \frac{\alpha_\infty}{0.73 + 0.083\sqrt{\alpha_\infty} + \alpha_\infty}\,, \qquad \alpha > \alpha_\infty\,, \tag{25}$$

which should be used in the sound-wave and MHD contributions in the case of runaway bubbles, in Eqs. (16) and (18), (19), respectively.

The minimal value of α for runaway bubbles,

$$\alpha_\infty \simeq \frac{15}{12\pi^2}\frac{\sum_i r_i n_i \Delta m_i^2(v_h(T_n))}{g_* T_n^2}\,, \qquad r_i = \begin{cases} 1 & \text{for bosons} \\ \frac{1}{2} & \text{for fermions} \end{cases} \tag{26}$$

is model-dependent, with the sum over all particles that are initially light (before the PT) and then become heavy in the final phase. Here, Δm_i correspond to the mass differences for each particle between the initial and final phases, and n_i is the number of d.o.f.'s for particle species i. For the case of the EWPT, a simple estimate taking into account the standard model particle content $\{W^\pm, Z, t\}$ gives [42]

$$\alpha_\infty \simeq 4.9 \times 10^{-3} \left(\frac{v_h(T_n)}{T_n}\right)^2\,. \tag{27}$$

V. TYPE I SEESAW MECHANISM: LOW AND HIGH SCALE

Having discussed the generic aspects of FOPTs and their link to primordial GW, let us now connect them to realistic models of particle physics which can explain small neutrino masses. The aim of this work is to explore the potential of upcoming gravitational wave experiments to probe and distinguish between some of the most popular neutrino mass generation mechanisms. In this section we give a brief review of the type-I seesaw models. We will focus on the various variants of type-I seesaw mechanism. We begin with discussion of high scale type-I seesaw mechanism before moving on to discuss one of its most interesting low scale variant, namely inverse seesaw mechanism. We will then discuss the dynamical "majoron variants" of both types of seesaw.

A. Minimal seesaw

Few steps allow to derive the minimal seesaw extension of the standard model. Within the latter, Dirac mass terms for charged leptons and quarks originate through tree level Yukawa couplings involving the Higgs doublet. The vacuum expectation value (vev) of the Higgs field then provides the Dirac masses to the standard model. As in the Type I seesaw mechanism, neutrino masses can be straightforwardly generated without affecting the renomarlizability of the theory through the introduction of right-handed neutrinos.

In what follows, we denote with e_{Li} the three left-handed charged lepton states, with e_{Ri} the right-handed charged lepton states, with ν_{Li} the three left-handed neutrino states, and with ν_{Li}^c their CP conjugates. We also introduce the

unitary transformations V, which act on the left-handed charged lepton fields E_L, the right-handed charged lepton fields E_R, and the left-handed neutrino fields ν_L, in order to realize the diagonal form with real eigenvalues

$$V^{E_L} m^E_{LR} V^{E_R\ \dagger} = \mathrm{diag}(m_e, m_\mu, m_\tau)\,, \tag{28}$$

$$V^{\nu_L} m_{LL} V^{\nu_L\ T} = \mathrm{diag}(m_1, m_2, m_3)\,. \tag{29}$$

Lepton mixing, realized by the matrix

$$\begin{pmatrix} \nu_e \\ \nu_\mu \\ \nu_\tau \end{pmatrix} = \begin{pmatrix} U_{e_1} & U_{e_2} & U_{e_3} \\ U_{\mu_1} & U_{\mu_2} & U_{\mu_3} \\ U_{\tau_1} & U_{\tau_2} & U_{\tau_3} \end{pmatrix} \begin{pmatrix} \nu_1 \\ \nu_2 \\ \nu_3 \end{pmatrix} \tag{30}$$

is finally recovered considering

$$U = V^{E_L} V^{\nu_L\,\dagger}\,.$$

Mass eigenstate neutrinos are denoted as ν_i, suppressing the subscript L.

The Lagrangian for the lepton sector of the standard model, with three right-handed neutrinos provided with heavy Majorana masses, casts

$$\mathcal{L}_{\rm mass} = -\epsilon_{ab}\left[\tilde{Y}^e_{ij} H^a_d L^b_i e^c_j - \tilde{Y}^\nu_{ij} H^a_u L^b_i \nu^c_j + \frac{1}{2}\nu^c_i \tilde{M}^{ij}_{RR} \nu^c_j\right] + \mathrm{h.c.}$$

where $\nu^p_{\rm R}$ have been replaced by their CP conjugates $\nu^c_{\rm i}$, $\tilde{M}^{ij}_{RR}$ denotes a complex symmetric Majorana matrix, and the Levi-Civita symbol $\epsilon_{ab} = -\epsilon_{ba}$ and $\epsilon_{12} = 1$ is used. Assigning to the two Higgs doublets[1] the vevs $\langle H^2_u \rangle = v_2$ and $\langle H^1_d \rangle = v_1$, the previous mass terms simplify to

$$\mathcal{L}_{\rm mass} = -v_1 \tilde{Y}^e_{ij} e_i e^c_j - v_2 \tilde{Y}^\nu_{ij} \nu_i \nu^c_j - \frac{1}{2}\tilde{M}^{ij}_{RR} \nu^c_i \nu^c_j + \mathrm{h.c.}\,.$$

In the matrix notation, once CP conjugates field have been replaced, this latter recasts

$$\mathcal{L}_{\rm mass} = -\bar{e}_L v_1 \tilde{Y}^{e\,*} e_R - \bar{\nu}_L v_2 \tilde{Y}^{\nu\,*} \nu_R - \frac{1}{2}\nu^T_R \tilde{M}^*_{RR}\, \nu_R + \mathrm{h.c.}\,.$$

A further simplification is obtained when switching to the diagonal charged lepton basis, $\mathrm{diag}(m_e, m_\mu, m_\tau) = V_{E_L} v_1 \tilde{Y}^{e\,*} V^\dagger_{E_R}$, and to the diagonal right-handed neutrino basis $\mathrm{diag}(M_1, M_2, M_3) = V_{\nu_R} \tilde{M}_{RR}{}^* V^T_{\nu_R}$, with V_{e_L}, V_{e_R} and V_{ν_R} unitary transformations. The neutrino Yukawa coupling then recast

$$Y^\nu = V_{E_L} \tilde{Y}^{\nu\,*} V^T_{\nu_R}\,, \tag{31}$$

and the Lagrangian is provided by

$$\begin{aligned} \mathcal{L}_{\rm mass} = &-(\bar{e}_L \bar{\mu}_L \bar{\tau}_L)\mathrm{diag}(m_e, m_\mu, m_\tau)(e_R \mu_R \tau_R)^T - (\bar{\nu}_{e_L} \bar{\nu}_{\mu_L} \bar{\nu}_{\tau_L}) Y^\nu\, v_2 (\nu_{R1}\nu_{R2}\nu_{R3})^T \\ &- (\nu_{R1}\nu_{R2}\nu_{R3})\mathrm{diag}(M_1, M_2, M_3)(\nu_{R1}\nu_{R2}\nu_{R3})^T + \mathrm{h.c.}\,. \end{aligned} \tag{32}$$

Right-handed neutrinos can be integrated out in the seesaw mechanism, hence recovering the neutrino mass Lagrangian

$$\mathcal{L}_{\rm mass} = -(\bar{e}_L \bar{\mu}_L \bar{\tau}_L)\mathrm{diag}(m_e, m_\mu, m_\tau)(e_R \mu_R \tau_R)^T - \frac{1}{2}(\bar{\nu}_{e_L} \bar{\nu}_{\mu_L} \bar{\nu}_{\tau_L}) m_{LL} (\nu^c_{e_L} \nu^c_{\mu_L} \nu^c_{\tau_L})^T + \mathrm{h.c.}\,. \tag{33}$$

Here the light effective left-handed Majorana neutrino mass matrix is provided by the seesaw formula

$$m_{LL} = -v_2^2\, Y^\nu \mathrm{diag}(M_1^{-1}, M_2^{-1}, M_3^{-1}) Y^{\nu\,T}\,. \tag{34}$$

---

[1] The way we present the standard model Lagrangian in terms of left-handed fields, replacing right-handed fields by their CP conjugates, and of two Higgs doublets, is particularly useful to pave the way for the supersymmetric standard model. The minimal seesaw model with one Higgs doublet can be recovered immediately setting one of the two Higgs doublets to be the charge conjugate of the other, namely $H_d \equiv H^c_u$.

This latter formula is equivalent to the low energy Lagrangian that involves the charged leptons and neutrino mass matrices

$$\mathcal{L}_{\rm mass} = -(\bar{e}_{L1}\,\bar{e}_{L2}\,\bar{e}_{L3})\,m^E_{LR}\,(e_{R1}\,e_{R2}\,e_{R3})^T - \frac{1}{2}(\bar{\nu}_{L1}\,\bar{\nu}_{L2}\,\bar{\nu}_{L3})\,m_{LL}\,(\nu^c_{L1}\nu^c_{L2}\nu^c_{L3})^T + \text{h.c.} \tag{35}$$

where m^E_{LR} and m_{LL} denote respectively a complex charged lepton mass matrix and a complex symmetric neutrino Majorana matrix, the eigenvalues of which provide the neutrino and charged lepton masses.

B. Simplest inverse seesaw

In the inverse seesaw model, the simplest standard model is extended by adding to the standard model isodoublet neutrinos (ν_i), three pairs of TeV scale of SU(2) singlet neutrinos (ν^c_i, S_i), with i denoting the family index running over $1, 2, 3$ [7, 8]. The S_i are charged under $\mathrm{U(1)_L}$ global lepton number with the same charge as the doublet neutrinos ν_i, i.e. $L(S) = +1$, but opposite to the lepton charge of the three ν^c_i, $L(\nu^c) = -1$.

The Yukawa terms relevant for neutrino mass generation are given by

$$\mathcal{L}^{\rm lept}_{\rm Yuk} = \mathcal{L}^{\rm SM}_{\rm Yuk} + Y_\nu \bar{L}^c \Phi \nu^c + M\nu^c S + \mu S S + \text{h.c.}\,, \tag{36}$$

where summation over the omitted flavor index i is assumed. The 3×3 matrices Y_ν and M represent the lepton number preserving Yukawa couplings and mass matrices respectively, while μ is the 3×3 matrix which violates the $U(1)_L$ symmetry. After electroweak (EW) symmetry breaking the Higgs gets a vacuum expectation value (vev) $\langle\Phi\rangle = v_h/\sqrt{2}$ one gets in the basis ν_i, ν^c_i, S_i, the mass matrix

$$\mathcal{M}_\nu = \begin{bmatrix} 0 & Y^T_\nu \langle\Phi\rangle & 0 \\ Y_\nu \langle\Phi\rangle & 0 & M^T \\ 0 & M & \mu \end{bmatrix}. \tag{37}$$

By using the general perturbative expansion method in [47, 48] one finds that, when the mass terms satisfy $M^{ij}_D, \mu^{ij} \ll M^{ij}$; $M^{ij}_D = Y^{ij}_\nu \langle\Phi\rangle$, the inverse seesaw mass matrix in Eq. (37) can be block–diagonalized so as to lead the effective light neutrino mass as

$$m_\nu{}^{\rm inverse} = M^T_D M^{T^{-1}} \mu M^{-1} M^*_D\,, \tag{38}$$

One sees that μ is the 3×3 Majorana mass matrix which triggers lepton number violation and is responsible for light neutrino mass generation. In the limit as $\mu \to 0$ the lepton number symmetry is restored, making the light neutrinos strictly massless. Thus the small neutrino mass follows in a natural way, in the sense of 't Hooft [49], as it is symmetry protected. The mass generation is illustrated by the Feynman diagram in Fig. 1. The heavy mainly isosinglet states

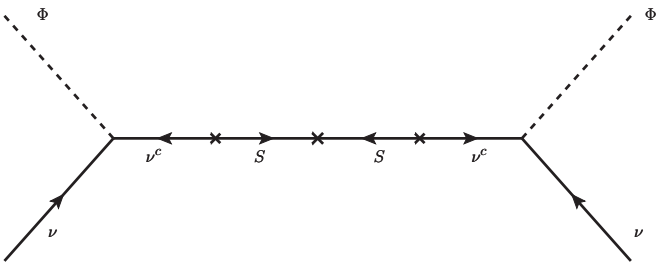

FIG. 1: Feynman diagram for the "inverse" seesaw mechanism with the explicit mass term.

form quasi-Dirac pairs with masses

$$m_{\nu^c,S} \simeq M \mp \frac{1}{2}\mu\,. \tag{39}$$

that can lie in the GeV-TeV range.

C. Minimal seesaw with majoron

We now turn to the possibility of generating dynamically the mass lepton number violation terms. For example, instead of introducing an explicit lepton number violation as the μ-term, one now assumes a $U(1)_L$ preserving extension of the standard model where not only the EW symmetry but also the $U(1)_L$ symmetry breaks spontaneously. For this purpose, the Higgs sector of the SM can be minimally extended by means of a new $SU(2)_L$ singlet complex scalar field σ with $U(1)_L$ assigned as $L(\sigma) = -2$.

D. Majoron inverse seesaw

Just like the Higgs sector of the SM can be minimally extended by means of a new $SU(2)_L$ singlet complex scalar field σ with $U(1)_L$ assigned as $L(\sigma) = -2$.[2]. It couples to the singlet neutrinos in a lepton number preserving way. The Yukawa term in Eq. 36 is now replaced by

$$\mathcal{L}^{\rm lept}_{\rm Yuk} = \mathcal{L}^{\rm SM}_{\rm Yuk} + Y_\nu \bar{L}^c \Phi \nu^c + M \nu^c S + Y_s S S \sigma + \text{h.c.}\,, \tag{40}$$

where as before we have suppressed the flavor index i of the fields. The vev of σ field breaks the lepton number symmetry $U(1)_L \to Z_2$ residual subgroup. Its breaking is associated with the generation of neutrino masses through the nonzero $\mu_{ij} S_i S_j$ mass terms. Here we assume that the μ term arises from the spontaneous lepton number violation in which case one has a majoron [50]. In contrast to the standard type I seesaw majoron the scale associated to the spontaneous lepton number violation is now relatively low, around the GeV-TeV scale.

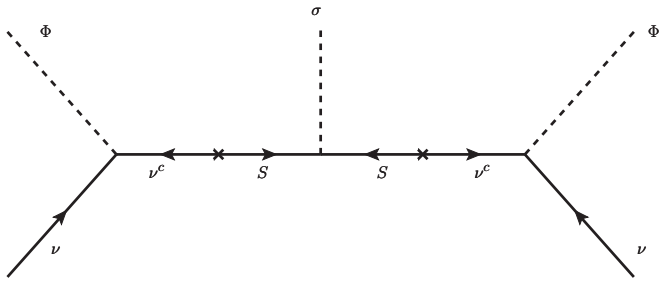

FIG. 2: Feynman diagram for the "inverse" seesaw mechanism with spontaneous lepton number violation by $\langle\sigma\rangle$.

The scalar potential of the majoron inverse seesaw model is given by

$$V_0(\Phi,\sigma) = \mu_\Phi^2 \Phi^\dagger\Phi + \lambda_\Phi (\Phi^\dagger\Phi)^2 + \mu_\sigma^2 \sigma^\dagger\sigma + \lambda_\sigma (\sigma^\dagger\sigma)^2 + \lambda_{\Phi\sigma} \Phi^\dagger\Phi\sigma^\dagger\sigma + \left(\frac{1}{2}\mu_b^2\sigma^2 + \text{h.c.}\right). \tag{41}$$

with Φ and σ given by

$$\Phi = \frac{1}{\sqrt{2}}\begin{pmatrix} G + iG' \\ \phi_h + h + i\eta \end{pmatrix}, \qquad \sigma = \frac{1}{\sqrt{2}}(\phi_\sigma + \sigma_R + i\sigma_I)\,, \tag{42}$$

with h, η, G, G', σ_R, σ_I being real scalars. The latter represent quantum fluctuations about the classical mean-fields $\phi_\alpha = \{\phi_h, \phi_\sigma\}$. In addition, for later convenience, in Eq. (41) we have also added a soft term (last term) which breaks $U(1)_L \to Z_2$ explicitly, giving a (small) pseudo-Goldstone mass to the imaginary part of field σ_I. The σ_I field is known as the "majoron" being the pseudo-Goldstone boson associated with Majorana mass generation for neutrions. We note that, under certain circumstances, the majoron can also be a viable Dark Matter candidae [13–19].

---

[2] Although unnecessary, in general, one can also obtain the invariant mass term M from a cubic Yukawa term, as in some string models.

E. Field-dependent tree-level mass spectrum at zero temperature

Before examining the finite temperature effects, let us now briefly discuss the field-dependent mass spectrum of the model at zero temperature. The scalar boson masses at zero temperature are determined as the eigenvalues of the Hessian matrix,

$$M^2_{\alpha\beta}(\phi_\alpha) = \frac{\partial^2 V}{\partial\phi_\alpha \partial\phi_\beta}\,, \tag{43}$$

for a given potential V. In our case only the electrically neutral real component of Φ and the real component of σ gets a non-zero vev, so the classical-field configurations in this case reads

$$\langle H^T\rangle = \frac{1}{\sqrt{2}}(0,\phi_h)\,, \qquad \langle S\rangle = \frac{\phi_\sigma}{\sqrt{2}}\,, \tag{44}$$

and the classical field-dependent (tree-level) potential is

$$V_0(\phi_h,\phi_\sigma) = \frac{\mu_h^2\phi_h^2}{2} + \frac{\lambda_h\phi_h^4}{4} + \frac{(\mu_\sigma^2+\mu_b^2)\phi_\sigma^2}{2} + \frac{\lambda_\sigma\phi_\sigma^4}{4} + \frac{\lambda_{\sigma h}\phi_h^2\phi_\sigma^2}{4}\,. \tag{45}$$

This potential is bounded from below (BFB) as long as the form is positive definite, so that the conditions

$$\lambda_h > 0\,, \qquad \lambda_\sigma > 0\,, \qquad 6\lambda_{\sigma h} > 0 \quad \text{or} \quad \lambda_{\sigma h} > -2\sqrt{\lambda_h\lambda_\sigma}\,, \tag{46}$$

are satisfied [3]. The tree-level perturbativity constraints require $\lambda_i < 4\pi$ for all the quartic couplings. However, keeping in mind the fact that this tree level potential will ultimately receive quantum as well as finite temperature corrections, we take a more conservative approach and in what follows, we rely on $|\lambda_i| < 5$ as the perturbativity constraint.

Given the potential in Eq. (45), it is straightforward to write down the field-dependent squared masses for CP-even states h and σ_R,

$$m^2_{h_1}(\phi_\alpha) = \frac{1}{2}(M^2_{hh} + M^2_{\sigma_R\sigma_R} - \sqrt{(M^2_{hh} - M^2_{\sigma_R\sigma_R})^2 + 4M^4_{h\sigma_R}})\,, \tag{47}$$

$$m^2_{h_2}(\phi_\alpha) = \frac{1}{2}(M^2_{hh} + M^2_{\sigma_R\sigma_R} + \sqrt{(M^2_{hh} - M^2_{\sigma_R\sigma_R})^2 + 4M^4_{h\sigma_R}})\,, \tag{48}$$

where the field-dependent M_{ij} elements are given by

$$M^2_{hh}(\phi_\alpha) = \mu_h^2 + 3\lambda_h\phi_h^2 + \frac{\lambda_{\sigma h}}{2}\phi_\sigma^2\,, \tag{49}$$

$$M^2_{\sigma_R\sigma_R}(\phi_\alpha) = \mu_\sigma^2 + \mu_b^2 + \frac{\lambda_{\sigma h}}{2}\phi_h^2 + 3\lambda_\sigma\phi_\sigma^2\,, \tag{50}$$

$$M^2_{h\sigma_R}(\phi_\alpha) = \lambda_{\sigma h}\phi_h\phi_\sigma\,, \tag{51}$$

where the last term is the only non-diagonal term in the CP-even scalar mass matrix. The field-dependent squared masses of the remaining scalar and Goldstone degrees of freedom read

$$m^2_G(\phi_\alpha) = m^2_{G'}(\phi_\alpha) = m^2_\eta(\phi_\alpha) = \mu_h^2 + \lambda_h\phi_h^2 + \frac{\lambda_{\sigma h}}{2}\phi_\sigma^2\,, \qquad m^2_{\sigma_I}(\phi_\alpha) = \mu_\sigma^2 - \mu_b^2 + \frac{\lambda_{\sigma h}}{2}\phi_h^2 + \lambda_\sigma\phi_\sigma^2\,. \tag{52}$$

On the other hand the zero temperature field-dependent gauge boson masses

$$m^2_Z(\phi_h) = \frac{\phi_h^2}{4}(g^2+g'^2)\,, \qquad m^2_{W^\pm}(\phi_h) = \frac{\phi_h^2}{4}g^2\,, \tag{53}$$

---

[3] Stability conditions in the context of the inverse seesaw majoron model were studied in Ref. [20–22].

are found as the eigenvalues of the $\{W_{1,2,3}, B\}$ mass matrix

$$M^2_{\rm gauge}(\phi_h) = \frac{\phi_h^2}{4}\begin{pmatrix} g^2 & 0 & 0 & 0 \\ 0 & g^2 & 0 & 0 \\ 0 & 0 & g^2 & -gg' \\ 0 & 0 & -gg' & g'^2 \end{pmatrix}, \tag{54}$$

where g and g' are the $SU(2)_L$ and $U(1)_Y$ standard model gauge couplings, respectively.

Finally, heavy field-dependent t, b-quark and τ-lepton masses are given by

$$m_{t,b,\tau}(\phi_h) = \frac{y_{t,b,\tau}\phi_h}{\sqrt{2}}\,, \tag{55}$$

while for neutrinos the light and heavy masses in Eqs. (38) and (39) generalize to

$$m_\nu{}^{\rm inverse}(\phi_h, \phi_\sigma) = M_D^T(\phi_h) M^{T^{-1}} \mu(\phi_\sigma) M^{-1} M_D^*((\phi_h)\,, \tag{56}$$

$$m_{\nu^c,S}(\phi_\sigma) \simeq M \mp \frac{1}{2}\mu(\phi_\sigma) \tag{57}$$

where $M_D(\phi_h)$ and $\mu(\phi_\sigma)$ are 3×3 field-dependent mass matrices and M is the 3×3 invariant mass matrix of Eq. (40). For the case where the lepton number symmetry $U(1)_L$ is explicitly broken at zero temperature, the field dependent $\mu(\phi_\sigma)$ matrix should be replaced by the invaraint 3×3 matrix μ i.e. $\mu(\phi_\sigma) \to \mu$. In the following sections we will consider both cases of explicit and spontaneous breaking of the lepton-number symmetry at zero temperature in more detail.

F. Explicitly vs spontaneously broken lepton number

We now discuss in more detail the cases of explicit and spontaneous $U(1)_L$ symmetry breaking. The classical mean-fields $\phi_\alpha = \{\phi_h, \phi_\sigma\}$ reach their vacuum expectation values in the minimum of a given potential V, for which in the zero-temperature limit $T \to 0$ we have

$$\Big\langle \frac{\partial V}{\partial \phi_\alpha} \Big\rangle_{\rm vac} = 0\,, \qquad \langle\phi_h\rangle_{\rm vac} \equiv v_h \simeq 246\,{\rm GeV}\,, \qquad \langle\phi_\sigma\rangle_{\rm vac} \equiv v_\sigma\,, \tag{58}$$

For a realistic model v_h must be non-zero as it gives mass to all quarks, charged leptons and gauge bosons. However, the vev of σ field can be either zero or non-zero. These cases will correspond to explicit and spontaneous $U(1)_L$ symmetry breaking, respectively. We consider both cases of $v_\sigma = 0$ and $v_\sigma \neq 0$ separateley.

Consider first the case of softly broken $U(1)_L$ and spontaneously broken EW symmetry, i.e. with $\mu_b \neq 0$, $\langle\phi_\sigma\rangle_{\rm vac} \equiv v_\sigma = 0$ and $\langle\phi_h\rangle_{\rm vac} \equiv v_h \neq 0$. In this case, the SM vacuum stability condition $\mu_h^2 = -\lambda_h v_h^2$ implies the presence of SM Higgs boson which does not mix with the other CP-even scalar so the mass matrix is already diagonal, i.e.

$$m_h^2 = 2\lambda_h v_h^2\,, \qquad m^2_{\sigma_R} = \mu_\sigma^2 + \mu_b^2 + \frac{\lambda_{\sigma h} v_h^2}{2}\,, \qquad m^2_{\sigma_I} = \mu_\sigma^2 - \mu_b^2 + \frac{\lambda_{\sigma h} v_h^2}{2}\,. \tag{59}$$

The $U(1)_L$ soft-breaking mass term, μ_b^2, thus introduces a mass splitting between the majoron σ_I and the second CP-even scalar σ_R. The majoron can still be a good dark matter candidate. In fact, for $\mu_b^2 > 0$, the majoron mass m_{σ_I} can be tuned to make it a viable dark matter candidate.

In practical calculations, it is convenient to use the scalar boson masses, $\lambda_{\sigma h}$ and the electroweak vev v_h as input parameters. The other parameters of the model can then be expressed in terms of these input parameters as

$$\lambda_h = \frac{m_h^2}{2v_h^2}\,, \qquad \mu_\sigma^2 = \frac{1}{2}(m^2_{\sigma_R} + m^2_{\sigma_I} - \lambda_{\sigma h} v_h^2)\,, \qquad \mu_b^2 = \frac{1}{2}(m^2_{\sigma_R} - m^2_{\sigma_I})\,. \tag{60}$$

In order to have a dynamical origin for the Majorana μ term in Eq. (36), we consider the case of a generic vacuum state with $v_h, v_\sigma \neq 0$. This is the case of spontaneously broken global $U(1)_L$ in the lepton sector, and the majoron

emerges in the physical spectrum as a Goldstone boson. A small but negative $\mu_b^2 < 0$ term then turns it to a physical pseudo-Goldstone state, with a small but non-zero mass protected from radiative corrections by an approximate $U(1)_L$ symmetry. Such a small-mass pseudo-Goldstone majoron is, again, potentially a very good candidate for light Dark Matter particle [13–19].

The minimization conditions for the vacuum state in this case are,

$$\mu_h^2 = -\lambda_h v_h^2 - \frac{1}{2}\lambda_{\sigma h} v_\sigma^2 \,, \qquad \mu_\sigma^2 = -\mu_b^2 - \lambda_\sigma v_\sigma^2 - \frac{1}{2}\lambda_{\sigma h} v_h^2 \,, \tag{61}$$

Using these tadpole conditions we get the 2×2 CP-even mass squared matrix expressed as

$$M^2_{\rm CP-even} = \begin{pmatrix} 2\lambda_h v_h^2 & \lambda_{\sigma h} v_h v_\sigma \\ \lambda_{\sigma h} v_h v_\sigma & 2\lambda_\sigma v_\sigma^2 \end{pmatrix} \,, \quad \mathcal{R} = \begin{pmatrix} \cos\theta & \sin\theta \\ -\sin\theta & \cos\theta \end{pmatrix} \,, \quad \begin{pmatrix} m_{h_1}^2 & 0 \\ 0 & m_{h_2}^2 \end{pmatrix} = \mathcal{R} M^2_{sh} \mathcal{R}^{-1} \,, \tag{62}$$

where the electroweak vev parameter is $v_h \simeq 246$ GeV one of the eigenvalues should be fixed to the SM-like Higgs boson mass, and $m_h \simeq 125$ GeV. Besides, a pseudo-Goldstone mass for the majoron satisfies

$$m_{\sigma_I}^2 = -2\mu_b^2 > 0. \tag{63}$$

The positive-definite scalar masses squared, together with the BFB conditions Eq. (46) ensure the vacuum stability in this scenario.

The scalar mass spectrum in the case of spontaneously broken $U(1)_L$ and SM gauge symmetries is readily obtained from Eq. (48), by taking the values of the mean-fields in the vacuum. It is, however, more convenient to represent the masses in terms of the (σ, h)-mixing angle, θ, introduced in Eq. (62) as follows

$$m^2_{h_1,h_2} = \lambda_h v_h^2 + \lambda_\sigma v_\sigma^2 \mp \frac{\lambda_\sigma v_\sigma^2 - \lambda_h v_h^2}{\cos 2\theta} \,. \tag{64}$$

In the two distinct decoupling cases,

$$\text{(I)} \quad v_h \ll v_\sigma : \qquad m_{h_1}^2 \simeq 2\lambda_h v_h^2 - \frac{\lambda_{\sigma h}^2 v_h^2}{2\lambda_\sigma} \equiv m_h^2 \,, \quad m_{h_2}^2 \simeq 2\lambda_\sigma v_\sigma^2 + \frac{\lambda_{\sigma h}^2 v_h^2}{2\lambda_\sigma} \,, \tag{65}$$

$$\text{(II)} \quad v_h \gg v_\sigma : \qquad m_{h_1}^2 \simeq 2\lambda_\sigma v_\sigma^2 - \frac{\lambda_{\sigma h}^2 v_\sigma^2}{2\lambda_h} \,, \quad m_{h_2}^2 \simeq 2\lambda_h v_h^2 + \frac{\lambda_{\sigma h}^2 v_\sigma^2}{2\lambda_h} \equiv m_h^2 \,, \tag{66}$$

such that depending on a particular hierarchy between the VEVs at $T = 0$ either m_{h_1} or m_{h_2} should be considered as the physical SM-like Higgs boson mass $m_h \simeq 125$ GeV. When both v_h and v_σ are at the EW scale, either choice is in principle possible, but in any case one must closely investigate the associated SM-like Higgs couplings to the gauge bosons and fermions in order to pick a phenomenologically consistent parameter-space point.

For practical purposes, it is convenient to choose the CP-even scalar boson masses, VEVs and the (σ, h)-mixing angle, θ, as input physical parameters (given at $T = 0$) and to express the scalar self-couplings as [**?**]

$$\lambda_\sigma = \frac{1}{4v_\sigma^2}\left(\cos 2\theta (m_{h_2}^2 - m_{h_1}^2) + m_{h_1}^2 + m_{h_2}^2\right) \,, \tag{67}$$

$$\lambda_h = \frac{1}{4v_h^2}\left(\cos 2\theta (m_{h_1}^2 - m_{h_2}^2) + m_{h_1}^2 + m_{h_2}^2\right) \,, \tag{68}$$

$$\lambda_{\sigma h} = \frac{1}{2v_h v_\sigma} \cos 2\theta \tan 2\theta (m_{h_2}^2 - m_{h_1}^2) \,, \tag{69}$$

For phenomenological consistency, one requires that the (σ, h)-mixing angle satisfies $|\cos\theta| > 0.85$, in order for the Higgs boson to have the SM-like couplings to the fermions and gauge bosons as suggested by the LHC data [20, 22]. The T-parameter from the global EW fit also sets stringent bounds on θ and on the mass of the CP-even Higgs partner m_σ. As was shown in Ref. [**?**], the bound on the mixing angle becomes stronger for larger m_{h_2}.

VI. EFFECTIVE INTERACTION POTENTIAL AT FINITE TEMPERATURE

In order to understand the main features of the phase transitions in the inverse seesaw majoron model, we need to study the thermal evolution of different vacua in a cooling universe. For this purpose, one introduces thermal corrections to the effective potential [51]. To one-loop order in perturbation theory, the effective potential has the following form [52, 53]

$$V_{\rm eff}(T) = V_0 + \Delta V^{(1)}(T) + V^{(1)}_{\rm CW} + V_{\rm ct}\,, \tag{70}$$

where the tree-level part V_0 is given by Eq. (45), $V^{(1)}_{\rm CW}$ is the zero-temperature Coleman-Weinberg (CW) potential at one-loop level, $V_{\rm ct}$ is the counterterm potential, and the $\Delta V^{(1)}(T)$ term accumulates the lowest-order (UV-finite) thermal corrections emerging at finite temperatures only.

The one-loop CW potential takes the standard form in Landau gauge,

$$V^{(1)}_{\rm CW} = \sum_i (-1)^{F_i} n_i \frac{m_i^4(\phi_\alpha)}{64\pi^2}\left(\log\left[\frac{m_i^2(\phi_\alpha)}{\Lambda^2}\right] - c_i\right)\,, \tag{71}$$

where $F = 0(1)$ for bosons (fermions), $m_i^2(\phi_\alpha)$ is the ϕ_α-field dependent mass of the particle i, n_i is the number of degrees of freedom (d.o.f.'s) for the particle i, Λ is a renormalization scale taken to be equal to the EW scale v_h relevant for the considering case of EW phase transitions, and, in the $\overline{\rm MS}$-renormalization scheme, the constant c_i is equal to 3/2 for each d.o.f. of scalars, fermions and longitudinally polarised gauge bosons, and to 1/2 for transversely polarised gauge bosons.

In practice, only heavy SM fermions and scalars have field-dependent masses and thus contribute to the evolution of the shape of the potential. While for the heavy sterile neutrinos ν^c, S, if their masses are much larger than the SM scale, $M_{ii} \gg v_h$, then they only add a constant to the potential and thus can be discarded in the consideration of the phase transitions. In their masses are less than or comparable to the the electroweak scale then their effects should also be taken into account. Moreover, one would naively think that the light neutrinos ν having masses $<< v_h$ scale will have negligible contribution. However, it should be noted that despite the small mass, thanks to the inverse seesaw mechanism, the Yuakwa coupling of light neutrinos to Higgs boson is not negligible. In fact it can be $\mathcal{O}(1)$ and can be the largest Yuakwa coupling in the model. Thus, the effect of light neutrino Yukawa coupling should also be taken into account.

The one-loop thermal corrections $\Delta V(T)$ read [52]:

$$\Delta V^{(1)}(T) = \frac{T^4}{2\pi^2}\left\{\sum_b n_b J_B\left[\frac{m_i^2(\phi_\alpha)}{T^2}\right] - \sum_f n_f J_F\left[\frac{m_i^2(\phi_\alpha)}{T^2}\right]\right\}\,, \qquad \Delta V^{(1)}(T=0) = 0\,, \tag{72}$$

where J_B and J_F are the thermal integrals for bosons and fermions, respectively, given by

$$J_{B/F}(y^2) = \int_0^\infty dx\, x^2 \log\left(1 \mp \exp[-\sqrt{x^2+y^2}]\right)\,, \tag{73}$$

whose high-temperature expansions $y \ll 1$ read

$$J_B(y^2) \simeq \frac{-\pi^4}{45} + \frac{\pi^2}{12}y^2 - \frac{\pi}{6}y^3 + \mathcal{O}(y^4)\,, \qquad J_F(y^2) \simeq \frac{7\pi^4}{360} - \frac{\pi^2}{24}y^2 + \mathcal{O}(y^4)\,. \tag{74}$$

In the first non-trivial order $y^2 \equiv (m/T)^2$, the thermal corrections can be written as follow

$$\Delta V^{(1)}(T) = \frac{T^2}{24}\left\{{\rm Tr}\left[M^2_{\alpha\beta}(\phi_\alpha)\right] + \sum_{i=W,Z,\gamma} n_i m_i^2(\phi_\alpha) + \sum_{i=t,b,\tau,N}\frac{n_i}{2} m_i^2(\phi_\alpha)\right\}\,, \tag{75}$$

where $M_{\alpha\beta}$ is the field-dependent scalar Hessian matrix, and the numbers of degrees of freedom for the vector bosons (W, Z and transversely polarised photon $A_T \equiv \gamma$), $(\bar{t}, \bar{b})$ t, b (anti)quarks, τ-lepton and sterile neutrinos are

$$n_W = 6, \qquad n_Z = 3, \qquad n_\gamma = 2, \qquad n_{t,b} = 12, \qquad n_\tau = 4, \qquad \nu = 6, \qquad n_\nu^c + n_S = 12\,. \tag{76}$$

In Eq. (75), all the field-independent terms are dropped out. Appearance of T^2-terms in the potential signals leads to symmetry restoration at high temperatures, while higher-order linear in T terms are responsible for a barrier between the high- and low-T phases. Provided that the trace of the Hessian in Eq. (75) is basis invariant, in the leading-order $\mathcal{O}(y^2)$ it is convenient to employ the gauge basis considering only diagonal elements of the scalar mass form. Therefore, the first-order thermal corrections of order T^2 affect only quadratic (in mean-fields) terms of the tree-level potential V_0 in Eq. (45) preserving its shape and changing the masses of the scalar fields only.

The symmetry restoration typically imply breakdown of perturbation theory such that a resummation of higher order diagrams is necessary. A standard way of accounting for higher-order corrections to all orders is to perform the resummation of the daisy diagrams [**?**]. The latter is achieved by adding the finite temperature corrections to the mass terms as follows

$$\mu_h^2(T) = \mu_h^2 + c_h T^2\,, \qquad \mu_\sigma^2(T) = \mu_\sigma^2 + c_\sigma T^2\,, \tag{77}$$

where $c_{h,\sigma}$ are found by considering the infrared limit of the corresponding two-point functions and take the form [**? ? ?**]

$$c_h = \frac{1}{8}g^2 + \frac{1}{16}(g^2 + g'^2) + \frac{1}{2}\lambda_h + \frac{1}{12}\lambda_{\sigma h} + \frac{1}{4}(y_t^2 + y_b^2) + \frac{1}{12}y_\tau^2 + \frac{1}{24}\kappa_\nu\,, \quad c_\sigma = \frac{1}{3}\lambda_\sigma + \frac{1}{6}\lambda_{\sigma h} + \frac{1}{24}\kappa_S\,, \tag{78}$$

where $\kappa_\nu \equiv \sum_{i=1}^3 y_{\nu_i}^2$ and $\kappa_S \equiv \sum_{i=1}^3 y_{S_i}^2$. The Yukawa couplings y_{ν_i} and y_{S_i} are as given in Eq. (40). Both Yukawa couplings can lead to pronounced thermal corrections. However, since we are interested in studying the effect of the majoron and the new fermions introduced in inverse seesaw mechanism, for simplicity and to highlight the role of σ and S fields, henceforth we will take $y_{\nu_i} << y_{S_i}$. We notice that the Yukawa couplings y_{S_i} affect the c_σ coefficient only, by means of a single free parameter κ_S, whose value for practical purposes can be chosen within a rather large interval, $\kappa_S = \{0.1 \ldots 10\}$. The thermal corrections are then universally introduced to the physical (field-dependent) scalar boson masses replacing $\{\mu_h, \mu_\sigma\}$ in Eqs. (49), (50) and (52) by the thermal mass terms $\{\mu_h(T), \mu_\sigma(T)\}$ given by Eq. (77). Note, beyond the leading order, such a simple form (75) with a trace of the Hessian does not hold any longer, and a full mass diagonalisation procedure of the one-loop effective potential with thermal mass terms (77) should be performed.

Analogically, the temperature dependence of the gauge boson masses at the leading-order is introduced by adding the T^2-corrections to the diagonal terms of the gauge boson mass form. Note, only longitudinally polarised gauge bosons receive thermal corrections. The corresponding $\{W_L^+, W_L^-, Z_L, A_L\}$ thermal masses are found by a diagonalisation of the following mass form

$$M^2_{\rm gauge}(\phi_h; T) = M^2_{\rm gauge}(\phi_h) + \frac{11}{6}T^2 \begin{pmatrix} g^2 & 0 & 0 & 0 \\ 0 & g^2 & 0 & 0 \\ 0 & 0 & g^2 & 0 \\ 0 & 0 & 0 & g'^2 \end{pmatrix}, \tag{79}$$

where the zero-temperature mass matrix $M^2_{\rm gauge}(\phi_h)$ is given in Eq. (54). While the mass of the transversely polarised photon, m_γ, is zero, the photon acquires a longitudinal polarisation A_L having a non-zero thermal (Debye) mass. The corresponding eigenvalues read

$$m^2_{W_L}(\phi_h; T) = m^2_W(\phi_h) + \frac{11}{6}g^2T^2\,, \qquad m^2_{Z_L, A_L}(\phi_h; T) = \frac{1}{2}m^2_Z(\phi_h) + \frac{11}{12}(g^2 + g'^2)T^2 \pm \mathcal{D}\,, \tag{80}$$

with background field-dependent W, Z boson masses given in Eq. (), and

$$\mathcal{D}^2 = \left(\frac{1}{2}m^2_Z(\phi_h) + \frac{11}{12}(g^2 + g'^2)T^2\right)^2 - \frac{11}{12}g^2g'^2T^2\left(\phi_h^2 + \frac{11}{3}T^2\right) \tag{81}$$

In general, due to the CW potential the VEVs and physical masses at $T = 0$ are shifted from their tree-level values. The counterterm potential $V_{\rm ct}$ in Eq. (70) is determined by the condition that the one-loop effective potential reproduces the measured physical value of Higgs boson mass, $m_h \simeq 125$ GeV, and the Higgs VEV, $v_h \simeq 246$ GeV, in the zero-temperature limit. Provided that the shifts in the scalar quartic couplings are typically very small $\delta\lambda \ll \lambda$, for simplicity of practical calculations, it is sufficient to compute the counterterms for the mass terms only as follows [54]

$$V_{\rm ct} = \frac{\delta\mu_h^2\phi_h^2}{2} + \frac{\delta\mu_\sigma^2\phi_\sigma^2}{2}\,, \qquad \delta\mu_h^2 = -\frac{1}{v_h}\,\frac{\partial V_{\rm CW}^{(1)}}{\partial\phi_h}\bigg|_{\rm vac}\,, \qquad \delta\mu_\sigma^2 = -\frac{1}{v_\sigma}\,\frac{\partial V_{\rm CW}^{(1)}}{\partial\phi_\sigma}\bigg|_{\rm vac}\,, \tag{82}$$

such that the tree-level mass formulas are preserved at $T = 0$.

The fixed-order quantum corrections necessarily lead to the renormalisation scale Λ dependence of the effective potential seen already in the one-loop CW potential in Eq. (71). In the considering case of EW phase transitions, the choice of the renormalisation scale Λ becomes particularly important when a given mass parameter is very different from the EW VEV v_h. In order to minimise the RG scale dependence, it is then instructive to switch to the so-called renormalisation group (RG) improved potential where the potential parameters are given by their running values evaluated at the RG scale Λ. In the current analysis of the EW PTs, however, it is sufficient to consider the values of the potential parameters fixed at the EW scale, $\Lambda = v_h \simeq 246$ GeV, provided that the considering scalar boson masses and phase transition temperatures are not very different from this value.

VII. NUMERICAL RESULTS

In this section we look at the GW originating from FOPT in the seesaw models. First this to note is that in the type-I seesaw FOPT and hence GW will not occur as mentioned before. However, in inverse seesaw as well as in Majoron extensions of the seesaw (type-I + Majoron result is awaited) we have the possibility of GW. In this section we discuss these possibilities

We calculate the saturated latent heat and compare it to the latent heat released by the transition. We consider that a bubble runs away if the amount of released latent heat is bigger than the saturated one. In most considered cases, the bubbles do not run away (??), while for a smaller fraction of those which do run away we use the proper procedure detailed in Ref. [42], and also briefly described in Appendix IV. In the case of non-runaway nucleated bubbles, the intensity of the GW radiation grows with the strength of the transition given by the ratio $v_h(T_n)/T_n$. Our calculations confirm the general expectation that for bubble wall velocities close to the speed of light, i.e. when $v_b \simeq 1$, the dominant component is the wall collision component, $h^2\Omega_{\rm coll}$, while our numerical results consistently take into account all the underlined GWs sources.

Let us consider ...

A. Majoron extension of type-I seesaw

B. Inverse Seesaw

The FOPT does indeed happens in inverse seesaw models, thanks to the presence of extra fermions in the model. However, since the fermions only contribute indirectly to the Higgs potential through loop corrections, the resulting GW are very weak and are completely out of reach of present and the planned future detectors. This can be seen from Fig. 3.

As can be seem from these plots, although the FOPT indeed occurs in inverse seesaw models but the resulting GW wave has too low an amplitude to be detected by any present or near future detector.

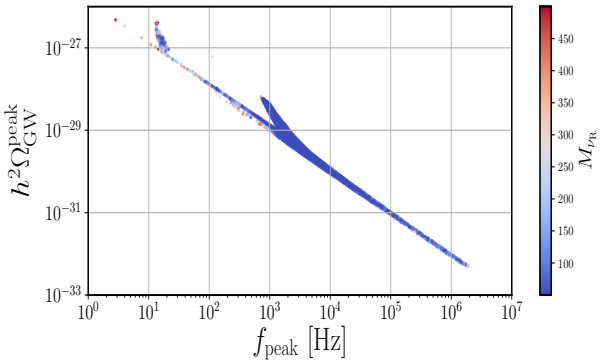

(a) Variation of GW amplitude and frequency with respect to the increase in mass of the heavy gauge singlet fermions ν^c, S. The plot is done for one generation of quassi degenerate fermions keeping the Yukawa coupling fixed. Parameter details in text.

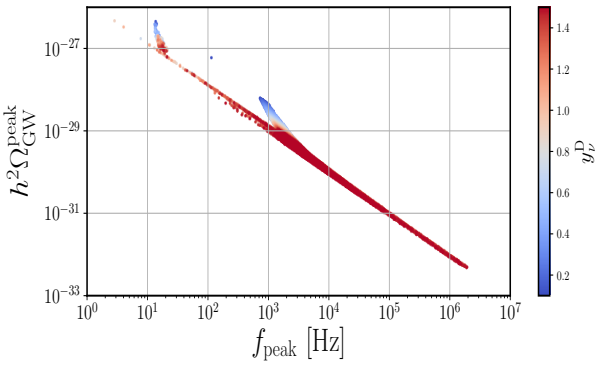

(b) Same as before but showing variation wrt the Yukawa coupling, keep the singlet fermion masses fixed.

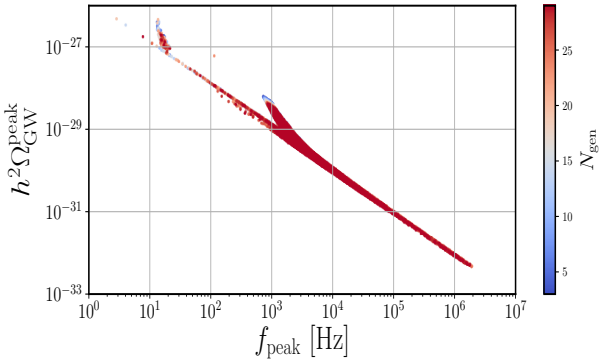

(c) Variation of GW amplitude and frequency when extra generations of singlet fermions are added. Such models with more than 3 gens of singlet fermions are over complete as more fermions are not needed from neutrino mass generation.

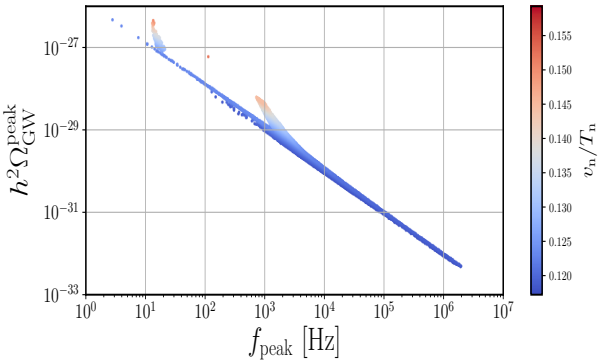

(d) Same as before but showing variation wrt the nucleation vev and nucleation temparature ratio.

FIG. 3: The GW amplitude and frequency in inverse seesaw, with respect to variation of various parameters of the model. In each plot one parameter of the model is varied keeping the other parameters fixed to a given benchmark value. See text for details

label	v_n/T_n	T_c	T_n	β/H	α	v_b
(1)	??	??	??	??	??	??
(2)	??	??	??	??	??	??

TABLE I: Properties of the transitions ...

C. Inverse Seesaw with Majoron

For the case of Majoron extension of inverse seesaw, the FOPT becomes very strong and GW are generated which can be detected in upcoming exp. Fig.4 shows the single peak GW for some chosen benchmark values.

One can see that in the Majoron extension of inverse seesaw one has very strong FOPT, leading to GW which are well within reach of upcoming experiments such as LISA. An even more attractive feature of our model is the presence

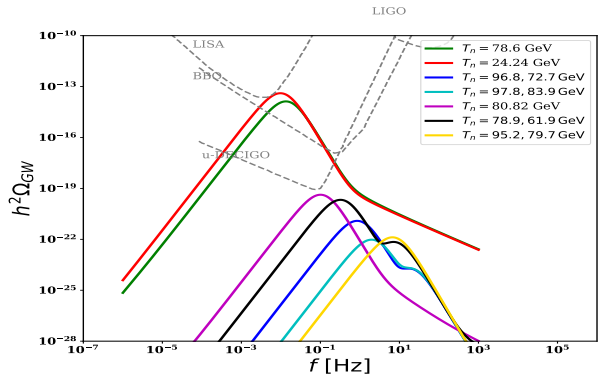

(a) Single peak GW spectrum for various benchmark values of nucleation temperature. Parameter details in text

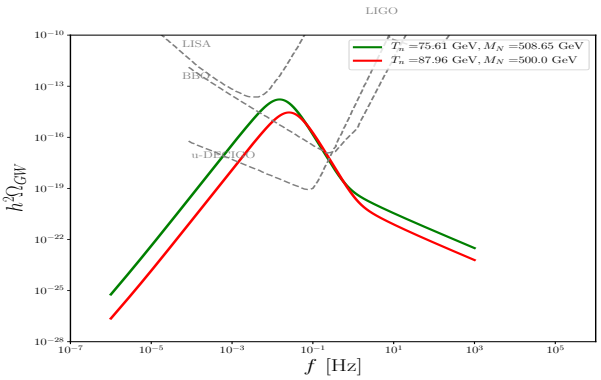

(b) Single peak GW spectrum for various benchmark values of nucleation temperature and mass of singlet fermion ν^c. Parameter details in text

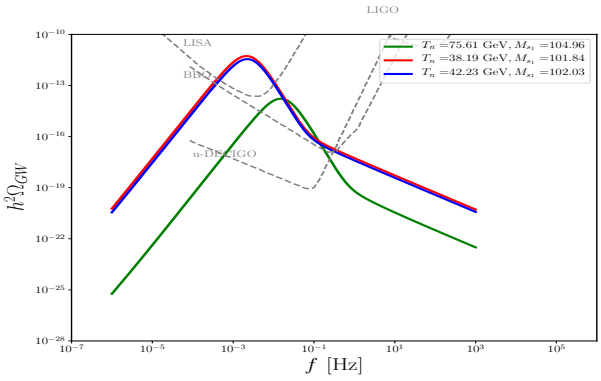

(c) Single peak GW spectrum for various benchmark values of nucleation temperature and mass of singlet fermion S.

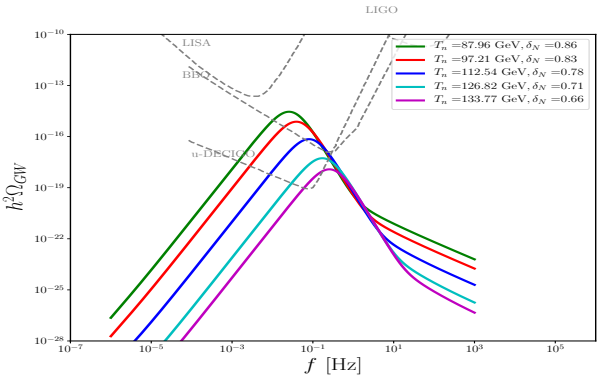

(d) Single peak GW spectrum for various benchmark values of nucleation temperature and the strength of $SS\sigma$ Yukawa coupling.

FIG. 4: The GW amplitude and frequency in the Majoron extension of inverse seesaw, with respect to variation of various parameters of the model. In each plot one parameter of the model is varied keeping the other parameters fixed to a given benchmark value. See text for details

of "double peak" gravitational waves as shown in Fig. **??** below.

It should be noted that this double peak feature is a generic prediction of the model and can happen for various different parameter choices of the model as shown in Fig. 6 below

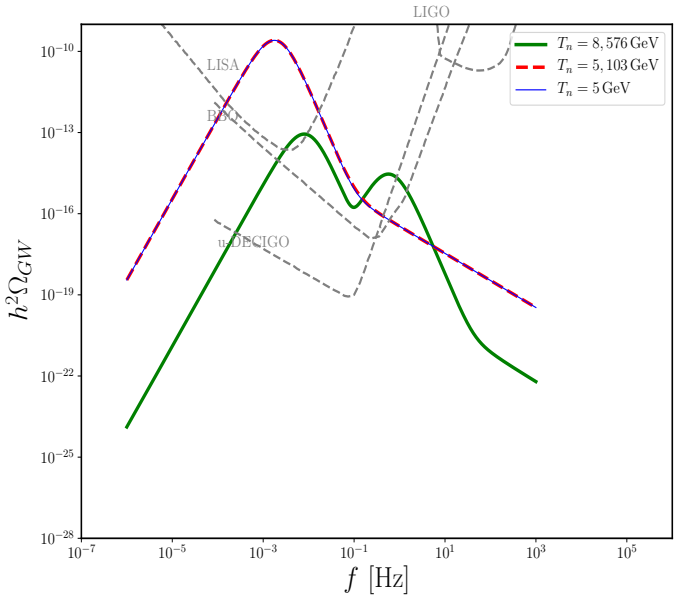

FIG. 5: The double peak gravitation wave spectrum in our model and the sensitivity reach of near future experiments. One can see that the double peak prediction of our model can be tested in near future experiments. Parameter details in text

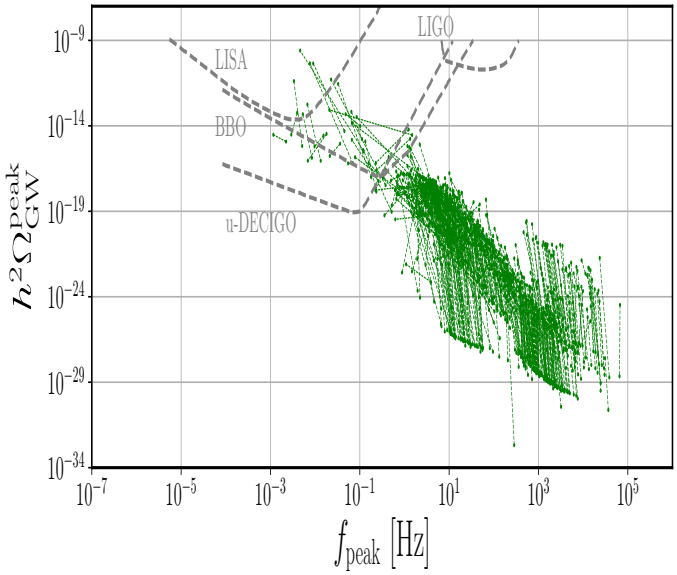

FIG. 6: The double peak gravitation wave spectrum in our model for different benchmark choices of parameters. The two ends of each line represent the location of the two peaks of the double peak GW spectrum. The two points of double peak are joined by a line to easily identify which two peaks are associated with each other.

VIII. SUMMARY AND CONCLUSIONS

The analysis we presented here deals with the most popular implementations of the Type-I see-saw mechanism that account to generate neutrinos' masses. Both the cases of explicit and spontaneous breakdown of the Lepton symmetry were addressed, the latter case being associated with the Majoron field. The Majoron field in turn retains much phenomenological interest, since it can account for dark matter. Our results enlightened that a channel for shedding light on neutrino mass generation can be provided, from a multi-messenger perspective, by the gravitational-wave physics. Specifically, we realized that different pattern of phase transitions allow to falsify various phenomenological

models, and found evidences that explicit lepton violations cannot induce any strong electroweak phase transition for all the see-saw type-I models. Consequently, any gravitational-wave background signal arises that is testable by the next-generation of satellite interferometers. Conversely, we discovered that a much phenomenologically reacher scenario can be provided by those models that, involving the Majoron, account for Lepton number violations and neutrinos' masses emerging from a dynamical mechanism. Within this case, we found that both the standard low scale model and the inverse Type-I see-saw model do predict strong gravitational wave signals. This is a prediction that can be tested in the $0.1 \div 100\,\mathrm{mHz}$ frequency range, and thus highly motivates future experimental proposals, among which LISA, U-DECIGO and BBO, that will probe the mHz frontier. What is also remarkable of this scenario, is that it entails an indirect and complementary way to falsify models of neutrino mass generation, as well as provides a relevant probe of the electroweak phase transition. Furthermore, for the sake of phenomenologically distinguishing the models under scrutiny, it is crucial that the two Type-I see-saw models that we considered, which hold spontaneously broken lepton number, actually produce GW spectra which differ from one another model.

ACKNOWLEDGMENTS

Useful discussions and helpful correspondence with Zurab Berezhiani, Yifu Cai and Nico Yunes are gratefully acknowledged. A.P.M wants to thank Marek Lewicki and Bogumila Świezewska for insightful discussions about bubble wall collision contributions to the spectrum of GW. A.A. and A.M. wish to acknowledge support by the NSFC, through grant No. 11875113, the Shanghai Municipality, through grant No. KBH1512299, and by Fudan University, through grant No. JJH1512105. J.B. acknowledges his partial support by the NSFC, through the grants No. 11375153 and 11675145. A.A. and A.M. would like to thank IFIC for hospitality during the preparation of this work. R.P. is supported in part by the Swedish Research Council grants, contract numbers 621-2013-4287 and 2016-05996, by CONICYT grant MEC80170112, as well as by the European Research Council (ERC) under the European Union's Horizon 2020 research and innovation programme (grant agreement No 668679). The work of R.P. was also supported in part by the Ministry of Education, Youth and Sports of the Czech Republic, project LT17018. The work of A.M. has been performed in the framework of COST Action CA16201 "Unraveling new physics at the LHC through the precision frontier" (PARTICLEFACE). R.V. and J.W.F.V. are supported by the Spanish grants SEV-2014-0398 and FPA2017-85216-P (AEI/FEDER, UE), PROMETEO/2018/165 (Generalitat Valenciana) and the Spanish Red Consolider MultiDark FPA2017-90566-REDC.

[1] T. Kajita, "Nobel Lecture: Discovery of atmospheric neutrino oscillations," *Rev.Mod.Phys.* **88** (2016) 030501.

[2] A. B. McDonald, "Nobel Lecture: The Sudbury Neutrino Observatory: Observation of flavor change for solar neutrinos," *Rev.Mod.Phys.* **88** (2016) 030502.

[3] A. Kosowsky, M. S. Turner, and R. Watkins, "Gravitational waves from first order cosmological phase transitions," *Phys. Rev. Lett.* **69** (1992) 2026–2029.

[4] J. W. F. Valle and J. C. Romao, *Neutrinos in high energy and astroparticle physics*. John Wiley & Sons (2015). www.wiley.com/buy/9783527411979.

[5] A. S. Joshipura and J. W. F. Valle, "Invisible higgs decays and neutrino physics," *Nuclear Physics B* **397** no. 1, (1993) 105 – 122. http://www.sciencedirect.com/science/article/pii/055032139390337O.

[6] S. M. Boucenna, S. Morisi, and J. W. F. Valle, "The low-scale approach to neutrino masses," *Adv.High Energy Phys.* **2014** (2014) 831598, arXiv:1404.3751 [hep-ph].

[7] R. Mohapatra and J. W. F. Valle, "Neutrino Mass and Baryon Number Nonconservation in Superstring Models," vol. D34, p. 1642. 1986.

[8] M. Gonzalez-Garcia and J. W. F. Valle, "Fast Decaying Neutrinos and Observable Flavor Violation in a New Class of Majoron Models," *Phys.Lett.* **B216** (1989) 360–366.

[9] E. K. Akhmedov *et al.*, "Left-right symmetry breaking in NJL approach," *Phys.Lett.* **B368** 270–280, arXiv:hep-ph/9507275 [hep-ph].

[10] E. K. Akhmedov *et al.*, "Dynamical left-right symmetry breaking," *Phys.Rev.* **D53** 2752–2780, arXiv:hep-ph/9509255 [hep-ph].

[11] M. Malinsky, J. Romao, and J. W. F. Valle, "Novel supersymmetric SO(10) seesaw mechanism," *Phys.Rev.Lett.* **95** 161801, arXiv:hep-ph/0506296 [hep-ph].

[12] C. Grojean and G. Servant, "Gravitational Waves from Phase Transitions at the Electroweak Scale and Beyond," *Phys. Rev.* **D75** (2007) 043507, arXiv:hep-ph/0607107 [hep-ph].

[13] V. Berezinsky and J. W. F. Valle, "The KeV majoron as a dark matter particle," *Phys. Lett.* **B318** (1993) 360–366, arXiv:hep-ph/9309214 [hep-ph].

[14] M. Lattanzi and J. W. F. Valle, "Decaying warm dark matter and neutrino masses," *Phys. Rev. Lett.* **99** (2007) 121301, arXiv:0705.2406 [astro-ph].

[15] F. Bazzocchi *et al.*, "X-ray photons from late-decaying majoron dark matter," *JCAP* **0808** (2008) 013, arXiv:0805.2372 [astro-ph].

[16] M. Lattanzi *et al.*, "Updated CMB, X- and gamma-ray constraints on Majoron dark matter," *Phys.Rev.* **D88** 063528, arXiv:1303.4685 [astro-ph.HE].

[17] M. Lattanzi, R. A. Lineros, and M. Taoso, "Connecting neutrino physics with dark matter," *New J. Phys.* **16** no. 12, (2014) 125012, arXiv:1406.0004 [hep-ph].

[18] J.-L. Kuo *et al.*, "Decaying warm dark matter and structure formation," *JCAP* **1812** no. 12, (2018) 026, arXiv:1803.05650 [astro-ph.CO].

[19] M. Reig, J. W. F. Valle, and M. Yamada, "Light majoron cold dark matter from topological defects and the formation of boson stars," arXiv:1905.01287 [hep-ph].

[20] C. Bonilla, R. M. Fonseca, and J. W. F. Valle, "Vacuum stability with spontaneous violation of lepton number," *Phys. Lett.* **B756** (2016) 345–349, arXiv:1506.04031 [hep-ph].

[21] C. Bonilla, J. W. F. Valle, and J. C. Romao, "Neutrino mass and invisible Higgs decays at the LHC," *Phys. Rev.* **D91** no. 11, (2015) 113015, arXiv:1502.01649 [hep-ph].

[22] C. Bonilla, J. C. Romao, and J. W. F. Valle, "Electroweak breaking and neutrino mass: invisible Higgs decays at the LHC (type II seesaw)," *New J. Phys.* **18** no. 3, (2016) 033033, arXiv:1511.07351 [hep-ph].

[23] J. W. F. Valle, "Resonant Oscillations of Massless Neutrinos in Matter," *Phys.Lett.* **B199** (1987) 432–436.

[24] H. Nunokawa *et al.*, "Resonant conversion of massless neutrinos in supernovae," *Phys.Rev.* **D54** (1996) 4356–4363.

[25] D. Grasso, H. Nunokawa, and J. W. F. Valle, "Pulsar velocities without neutrino mass," *Phys.Rev.Lett.* **81** (1998) 2412–2415.

[26] A. Esteban-Pretel, R. Tomas, and J. W. F. Valle, "Probing non-standard neutrino interactions with supernova neutrinos," *Phys.Rev.* **D76** (2007) 053001, arXiv:0704.0032 [hep-ph].

[27] A. Esteban-Pretel, R. Tomas, and J. W. F. Valle, "Interplay between collective effects and non-standard neutrino interactions of supernova neutrinos," *Phys.Rev.* **D81** (2010) 063003, arXiv:0909.2196 [hep-ph].

[28] Z. Berezhiani, A. Smirnov, and J. W. F. Valle, "Observable Majoron emission in neutrinoless double beta decay," *Phys.Lett.* **B291** (1992) 99–105.

[29] J. Bernabeu *et al.*, "Lepton flavor nonconservation at high-energies in a superstring inspired standard model," *Phys. Lett.* **B187** 303.

[30] A. Ilakovac and A. Pilaftsis, "Flavor violating charged lepton decays in seesaw-type models," *Nucl. Phys.* **B437** (1995) 491, arXiv:hep-ph/9403398 [hep-ph].

[31] F. Deppisch and J. W. F. Valle, "Enhanced lepton flavour violation in the supersymmetric inverse seesaw model," *Phys. Rev.* **D72** 036001, hep-ph/0406040.

[32] F. Deppisch, T. S. Kosmas, and J. W. F. Valle, "Enhanced mu- e- conversion in nuclei in the inverse seesaw model," *Nucl. Phys.* **B752** 80–92, hep-ph/0512360.

[33] E. Arganda, M. Herrero, X. Marcano, and C. Weiland, "Imprints of massive inverse seesaw model neutrinos in lepton flavor violating Higgs boson decays," *Phys.Rev.* **D91** (2015) 015001, arXiv:1405.4300 [hep-ph].

[34] F. F. Deppisch, P. Bhupal Dev, and A. Pilaftsis, "Neutrinos and Collider Physics," *New J.Phys.* **17** (2015) 075019, arXiv:1502.06541 [hep-ph].

[35] F. F. Deppisch, N. Desai, and J. W. F. Valle, "Is charged lepton flavor violation a high energy phenomenon?," *Phys.Rev.* **D89** (2014) 051302, arXiv:1308.6789 [hep-ph].

[36] A. Linde, "Decay of the false vacuum at finite temperature," *Nuclear Physics B* **216** no. 2, (1983) 421 – 445. http://www.sciencedirect.com/science/article/pii/0550321383902936.

[37] M. Dine, R. G. Leigh, P. Y. Huet, A. D. Linde, and D. A. Linde, "Towards the theory of the electroweak phase transition," *Phys. Rev.* **D46** (1992) 550–571, arXiv:hep-ph/9203203 [hep-ph].

[38] S. R. Coleman, "The Fate of the False Vacuum. 1. Semiclassical Theory," *Phys. Rev.* **D15** (1977) 2929–2936. [Erratum: Phys. Rev.D16,1248(1977)].

[39] C. L. Wainwright, "CosmoTransitions: Computing Cosmological Phase Transition Temperatures and Bubble Profiles with Multiple Fields," *Comput. Phys. Commun.* **183** (2012) 2006–2013, arXiv:1109.4189 [hep-ph].

[40] G. Kurup and M. Perelstein, "Dynamics of Electroweak Phase Transition In Singlet-Scalar Extension of the Standard Model," *Phys. Rev.* **D96** (2017) 015036, arXiv:1704.03381 [hep-ph].

[41] L. Leitao and A. Megevand, "Gravitational waves from a very strong electroweak phase transition," *JCAP* **1605** no. 05, (2016) 037, arXiv:1512.08962 [astro-ph.CO].

[42] C. Caprini *et al.*, "Science with the space-based interferometer eLISA. II: Gravitational waves from cosmological phase transitions," *JCAP* **1604** no. 04, (2016) 001, arXiv:1512.06239 [astro-ph.CO].

[43] R. Jinno and M. Takimoto, "Gravitational waves from bubble collisions: An analytic derivation," *Phys. Rev.* **D95** no. 2, (2017) 024009, arXiv:1605.01403 [astro-ph.CO].

[44] M. Hindmarsh, S. J. Huber, K. Rummukainen, and D. J. Weir, "Gravitational waves from the sound of a first order phase transition," *Phys. Rev. Lett.* **112** (2014) 041301, arXiv:1304.2433 [hep-ph].

[45] C. Caprini, R. Durrer, and G. Servant, "The stochastic gravitational wave background from turbulence and magnetic fields generated by a first-order phase transition," *JCAP* **0912** (2009) 024, arXiv:0909.0622 [astro-ph.CO].

[46] A. Beniwal, M. Lewicki, J. D. Wells, M. White, and A. G. Williams, "Gravitational wave, collider and dark matter signals from a scalar singlet electroweak baryogenesis," arXiv:1702.06124 [hep-ph].

[47] J. Schechter and J. W. F. Valle, "Neutrino Masses in SU(2) x U(1) Theories," *Phys.Rev.* **D22** (1980) 2227.

[48] J. Schechter and J. W. F. Valle, "Neutrino decay and spontaneous violation of lepton number," *Phys. Rev. D* **25** (Feb, 1982) 774–783. https://link.aps.org/doi/10.1103/PhysRevD.25.774.

[49] G. t'Hooft *Ed. by E. Farhi et al. (World Scientific, Singapore). Cambridge* 345–367. Lectures at Cargese Summer Inst. 1979.

[50] M. C. Gonzalez-Garcia and J. W. F. Valle, "Fast decaying neutrinos and observable flavor violation in a new class of Majoron models," *Phys. Lett.* **B216** 360.

[51] L. Dolan and R. Jackiw, "Symmetry Behavior at Finite Temperature," *Phys. Rev.* **D9** (1974) 3320–3341.

[52] M. Quiros, "Finite temperature field theory and phase transitions," *Proceedings of Summer School in High-Energy Physics and Cosmology: Trieste, Italy, June 29-July 17, 1998* (1999) 187–259, arXiv:hep-ph/9901312 [hep-ph].

[53] D. Curtin, P. Meade, and H. Ramani, "Thermal Resummation and Phase Transitions," *Eur. Phys. J.* **C78** no. 9, (2018) 787, arXiv:1612.00466 [hep-ph].

[54] M. Jiang, L. Bian, W. Huang, and J. Shu, "Impact of a complex singlet: Electroweak baryogenesis and dark matter," *Phys. Rev.* **D93** no. 6, (2016) 065032, arXiv:1502.07574 [hep-ph].